European Journal of Nuclear Medicine and Molecular Imaging (2019) 46:1822–1829
https://doi.org/10.1007/s00259-019-04349-w

ORIGINAL ARTICLE

Head-to-head comparison of ^{11}C-PBR28 and ^{11}C-ER176 for quantification of the translocator protein in the human brain

Paolo Zanotti-Fregonara[1] · Belen Pascual[1] · Mattia Veronese[2] · Meixiang Yu[1] · David Beers[1] · Stanley H. Appel[1] · Joseph C. Masdeu[1]

Received: 7 February 2019 / Accepted: 29 April 2019 / Published online: 31 May 2019

Abstract

Introduction ^{11}C-ER176 is a new PET tracer to quantify the translocator protein (TSPO), a biomarker for inflammation. The aim of this study was to perform a head-to-head comparison between ^{11}C-ER176 and the widely used ^{11}C-PBR28.

Methods Seven healthy volunteers had a 90-min PET scan and metabolite-corrected arterial input function with ^{11}C-PBR28 in the morning and ^{11}C-ER176 in the afternoon. Binding was quantified at the regional level in terms of V_T with a two-tissue compartmental model. By using V_{ND} values from the literature obtained with pharmacological blockade, we derived the binding potential BP_{ND} for both tracers.

Results ^{11}C-ER176 was more stable in arterial blood than ^{11}C-PBR28 (the percentages of unmetabolized parent in plasma at 90 min were 29.0 ± 8.3% and 8.8 ± 2.9% respectively). The brain time–activity curves for both tracers were well fitted by the two-tissue model, but ^{11}C-ER176 had higher V_T values than ^{11}C-PBR28 (5.74 ± 1.54 vs 4.43 ± 1.99 ml/cm^3) and a lower coefficient of variation. The BP_{ND} of ^{11}C-ER176 was more than 4 times larger than that of ^{11}C-PBR28 for high-affinity binders, and more than 9 times larger for mixed-affinity binders.

Conclusion ^{11}C-ER176 displays a higher binding potential and a smaller variability of V_T values. Thanks to these characteristics, clinical studies performed with ^{11}C-ER176 are expected to have higher statistical power and thus require fewer subjects.

Keywords ^{11}C-PBR28 · ^{11}C-ER176 · TSPO · PET

Introduction

Dozens of positron emission tomography (PET) tracers for TSPO, a putative biomarker for inflammation, have been synthesized in the last 30 years [1]. On one hand, this reflects the interest in TSPO imaging, which has been employed to study conditions as disparate as Alzheimer's disease [2], major depression [3], schizophrenia [4], epilepsy [5], rheumatoid arthritis [6], and tumors [7]. On the other hand, perhaps, this also reflects the fact that the ideal TSPO tracer has not been found yet. For instance, the binding affinity of TSPO tracers is sensitive to a particular single-aminoacid polymorphism (rs6971) of the target protein [8]. Therefore, subjects who display a low binding affinity cannot be imaged with most tracers, which is detrimental especially to protocols on rare diseases and when patient recruitment is difficult. Also, the degrees of binding affinity of the remaining subjects must be accounted for statistically, thus reducing the statistical power of the study [9].

Despite the wealth of available tracers, only a handful of them have been well characterized in humans and used in research protocols [1]. Reaching a consensus about the ligand with the best imaging properties in humans would make it possible to use the imaging tool with the highest sensitivity and to pool subjects from different institutions.

However, comparing the relative qualities among tracers on the basis of the published literature is difficult, due to the use of different populations of subjects and different analytical

This article is part of the Topical Collection on Neurology.

✉ Paolo Zanotti-Fregonara
pzanottifregonara@houstonmethodist.org

[1] Nantz National Alzheimer Center and Houston Methodist Research Neurological Institute, and Weill Cornell Medicine, 6670 Bertner Ave, Houston, TX 77030, USA

[2] Department of Neuroimaging, Institute of Psychiatry, Psychology and Neuroscience, King's College London, London, UK

methods and endpoints [1]. Head-to-head protocols in the same subjects using full kinetic modeling would clearly provide the highest level of evidence of the relative properties of different tracers, but these studies are exceedingly rare. In what was probably the only study with this design for TSPO tracers, we recently showed that ^{18}F-GE180 has unfavorable characteristics for brain imaging compared to ^{11}C-PBR28, essentially because of its poor penetration of the blood–brain barrier and because of its high vascular signal, [10, 11].

In the present study, we compared ^{11}C-PBR28 [12] and ^{11}C-ER176, a recent TSPO radioligand characterized by a very high specific binding [13, 14], by scanning during the same day seven healthy subjects with both tracers.

Methods

Subjects

We studied seven healthy subjects (two men and five women; age 67.7 ± 5.0, range 60–74 years) recruited in 2018 at the Nantz National Alzheimer Center of the Houston Methodist Neurological Institute. Four subjects (including one of the men) were mixed-affinity binders (MABs) and three were high-affinity binders (HABs). Medical, neurological, and psychiatric disorders had been ruled out by a detailed history and physical, neurological, and neuropsychological examinations, as well as urine and blood tests, and electrocardiogram. All subjects had signed a written consent form, which had been approved by the Institutional Review Board of Houston Methodist Research Institute.

Brain imaging

On the bed of a Philips Gemini TF 64 scanner, subjects had their head encased by a thermoplastic pillow and mask to prevent movements. Vital signs were recorded before the injection of the tracer and at the end of the scan. A computed tomography scan was obtained first for attenuation correction. Then, the subjects were injected first with 743 ± 56 MBq of ^{11}C-PBR28 and, at least 3 h later to allow for radioactive decay and biological removal, with 723 ± 85 MBq of ^{11}C-ER176. Both tracers were given at the same time of the day in all subjects, to minimize potential variations due to circadian rhythms [15]. Injections were done over 1 min with an automated pump and were followed by a 90-min dynamic scan. A T1-weighted structural magnetic resonance imaging (MRI) scan was obtained for each subject using a 3-dimensional magnetization-prepared rapid gradient-echo pulse sequence with an echo time of 3.04 ms, repetition time of 7.648 ms, inversion time of 900 ms, and flip angle of 8° on a 3-T whole-body scanner (Discovery, GE Medical Systems) with a Nova 32-channel phased-array head coil. The PET dynamic frames were corrected for movement and coregistered to the structural MRI. Time–activity curves were obtained for 79 brain regions of interest (ROIs) of the Hammersmith atlas [16], as implemented in the Pneuro module of Pmod 3.9 (Zurich, Switzerland).

Measurement of the input functions

One radial catheter was placed in the morning and used to draw blood samples for both PET scans. The sampling schedule was the same for both tracers, and included 24 samples drawn every 15 s, and then at 4, 5, 6, 8, 10, 15, 20, 30, 40, 50, 60, 75, and 90 min. Samples were centrifuged to separate the plasma from the blood cells, and high-performance liquid chromatography was used to measure the concentration of radiometabolites in the plasma samples acquired at 5, 10, 15, 20, 30, 40, 50, 60, 75, and 90 min. The measured fractions of parent were fitted with an extended Hill function [17], and the parent concentrations were obtained by multiplying the parent fraction by the total plasma activity. The plasma free fraction was measured in duplicate by ultrafiltration [18] and normalized using a standard derived from donor plasma [19].

Image quantification

A two-tissue compartment model (2TCM) was used to derive the total volume of distribution (V_T), with the blood volume (V_B) estimated along with the other microparameters. The parent curves were fitted with a tri-exponential function after relative weighting, and the delay of the first pass of the tracer in the brain was corrected by fitting the whole grey matter. The whole blood time–activity curve was used to correct for the activity in the vascular compartment. Brain data were weighted by assuming that the standard deviation of the data was proportional to the inverse square root of the counts in the whole grey matter [20]. Kinetic modeling was done with Pmod 3.9 (Zurich, Switzerland).

Covariance analysis Comparison of tracer spatial variance was done using the Krzanowski test on the principal components to investigate the equality of their eigenvectors and eigenvalues of the tracer PET adjacency matrixes [21]. For each tracer, the corresponding adjacency matrix was defined as the population covariance matrix, where the correlation of the tracer V_T estimates for each couple of ROIs is computed across all the subjects [22]. The method was implemented by using the NetPET package (https://www.nitrc.org/projects/netpet_2018/) with its default settings (i.e., no thresholding and 10,000 permutations).

Estimation of the binding potential over the nondisplaceable compartment (BP_{ND})

BP_{ND} is defined as the ratio at equilibrium of specifically bound radioligand to that of nondisplaceable radioligand in

tissue [23], and equals the ratio of V_S (= V_T - V_{ND}) to V_{ND}. We estimated V_{ND} using two variations of the Lassen plot [24], namely, the genomic plot [25, 26] and the polymorphism plot [27].

Genomic plot Following the approach presented in [28], we considered the TSPO mRNA mappings from the Allen Human Brain Atlas [29] as a surrogate measure of specific binding, and we compared them with the regional V_T estimates for both tracers. Under the assumption that mRNA expression is predictive of in-vivo protein density of unrelated normal subjects, we evaluated whether the regional tracer uptakes were consistent with TSPO brain gene profiles. The comparison was performed by correlation analysis at the region level within the same regions considered for the PET quantification. The squared Pearson's coefficient (r^2) was used to quantify the linear correlation between the gene transcript and V_T. The x-intercept of the regression line provided an estimate of V_{ND}. The processing of the mRNA data was done with MENGA (Multimodal Environment for Neuroimaging and Genomic Analysis) [30].

Polymorphism plot This plot takes advantage of the polymorphism expressed by the TSPO protein to model the difference in the HAB and MAB signals in the context of an occupancy plot [27]. Assuming that the nonspecific binding is the same in both populations, the V_{ND} can be estimated by linearly regressing the V_T values of HABs vs MABs. Similarly to the genomic plot, the intercept on the x-axis identifies V_{ND}.

The V_{ND} obtained with these two approaches was compared to the ones known from studies with pharmacological blockade [14, 31].

Results

Plasma input functions

Both tracers peaked in plasma about 1–1.5 min after injection, although the peak standard uptake value (SUV) of the parent was higher for ^{11}C-PBR28 than for ^{11}C-ER716 (13.3 ± 1.9 vs 9.7 ± 3.5; $p = 0.009$). At 60 min, the SUV concentrations were 0.15 ± 0.06 for both tracers (Fig. 1). The percentage coefficient of variation (%COV: SD/mean * 100) of the areas under the curve of the parent was lower for ^{11}C-ER176 than for ^{11}C-PBR28 (24.6% vs 32.2%). The metabolism rate in plasma was faster for ^{11}C-PBR28 than for ^{11}C-ER716: at 90 min, the percentages of unmetabolized parent were 8.8 ± 2.9% and 29.0 ± 8.3%, respectively (Fig. 1).

The plasma free fractions were 4.9 ± 0.8% for ^{11}C-PBR28 and 5.4 ± 1.6% for ^{11}C-ER176. Notably, the higher value and higher standard deviation for ^{11}C-ER176 were due only to the presence of one subject with a high value (8.6%). Without this subject, the plasma free fraction of ^{11}C-ER176 would be 4.9 ± 0.9%.

Image quantification

Both tracers showed a high uptake in the brain (Fig. 2), especially ^{11}C-ER176: the time–activity curves of the whole brain peaked at about 8–10 min after injection, and were 1.85 ± 0.22 for ^{11}C-PBR28 and 2.13 ± 0.16 for ^{11}C-ER176. Similarly, the SUV data measured at 90 min after wash-out were 0.93 ± 0.19 for ^{11}C-PBR28 and 1.19 ± 0.16 for ^{11}C-ER176 (Fig. 3). The %COV of the areas under the curve of the whole brain was 8.2% for ^{11}C-ER176 and 14.1% for ^{11}C-PBR28.

With a 2TCM, out of a total of 553 brain regions (79 per patient), ^{11}C-PBR28 did not converge in only two regions, and showed a standard error (SE) greater than 20% in 17 other regions. These were mostly very small and noisy regions which are part of the Hammersmith atlas, such as the subcallosal area or the substantia nigra. Similarly, ^{11}C-ER176 did not converge in four regions, and the SE was larger than 20% in 16 other regions (here again, predominantly small regions that are rarely used as independent outcome measurements). V_T values (including all the regions that converged and whose SE was < 20%) were higher for ^{11}C-ER176 than for ^{11}C-PBR28 (Table 1), both on average and for each individual subject, but had similar SE and were well correlated between the two tracers ($R^2 = 0.80$; $p < 0.0001$). In agreement with the lower variability of both plasma and brain time–activity curves, the %COV of the V_T values were consistently lower for ^{11}C-ER176 than for ^{11}C-PBR28 (Table 1). The comparison of the 2TCM-derived microparameters shows slightly higher values of K_1 and k_3 for ^{11}C-ER176, compatible with an easier transfer to the brain from the vascular compartment and a higher binding to the TSPO receptor (Table 2).

Krzanowski tests on eigenvectors and eigenvalues did not show any statistical difference ($p_{eigenvector}$: 0.15, $p_{eigenvalue}$: 0.14, $\lambda = 19.07$, $\mu = 14.95$), which suggests that the distribution of the tracer uptake across brain regions is similar.

Estimation of binding potential relative to nondisplaceable uptake (BP_{ND})

Genomic plot For ^{11}C-PBR28, the mRNA and VT values were significantly correlated ($r^2 = 0.737$, $p = 0.0004$ for MABs and $r^2 = 0.403$, $p = 0.0265$ for HABs) (Fig 4a). The x-intercepts were 1.7 and 2.5 ml/cm^3, respectively, which compare favorably to the average value of 1.98 ml/cm^3 reported in the literature [31]. By contrast, for ^{11}C-ER176 the correlation between mRNA and VT values was significant only for MABs ($r^2 = 0.742$, $p = 0.0003$), but the estimated VND (2.35 ml/cm^3) was

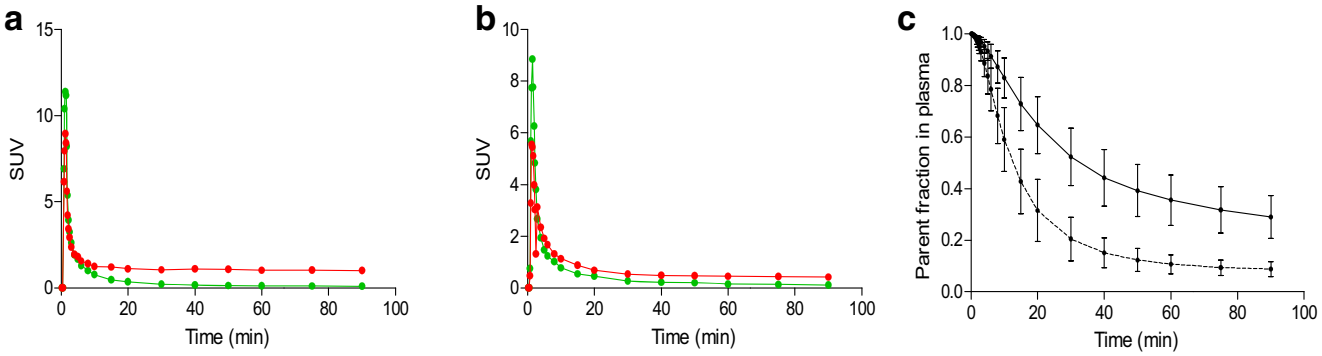

Fig. 1 SUV concentrations of the parent compound (*green lines*) and the whole blood (*red lines*) for ^{11}C-PBR28 (**a**) and ^{11}C-ER176 (**b**) in a representative subject. Both sets of curves are well-fitted by a triexponential function. Panel **c** shows the average and standard deviation from all subjects of the parent fraction in plasma for ^{11}C-PBR28 (*dashed line*) and ^{11}C-ER176 (*solid line*). ^{11}C-ER176 has a slower metabolism, as the parent constitutes about 30% of the total plasma activity at the end of the 90-min scan, while for ^{11}C-PBR28 it is generally < 10%

incompatible with the value known from studies with pharmacological blockade (0.65 ml/cm^3) (Fig. 4b). The r^2 for ^{11}C-ER176 HABs was 0.128 and non-significant.

Polymorphism plot The estimated V_{ND} for ^{11}C-PBR28 was 1.76 ml/cm^3 ($R^2 = 0.718$, $p < 0.0001$) (Fig. 4c), which is similar to the value of 1.98 ml/cm^3 reported in the literature [31]. Conversely, the fitting for ^{11}C-ER176 was very poor ($R^2 = 0.043$) (Fig. 4d) and the estimated V_{ND} value of 1.23 ml/cm^3 differed substantially from the V_{ND} value of 0.65 ml/cm^3 [14]. Therefore, for the sake of consistency, we used the V_{ND} values from the literature to calculate BP_{ND} for both tracers. The BP_{ND} of ^{11}C-ER176 was more than 4 times larger than that of ^{11}C-PBR28 for HAB and more than 9 times larger for MABs (Table 3).

Discussion

In this study, and consistently with previous studies on the kinetic modeling of both tracers [12, 14], we showed that both ^{11}C-PBR28 and ^{11}C-ER716 show a high uptake and fast washout from the brain, well fitted by a 2TCM. The V_T values of both tracers were well correlated and covariance analysis showed a similar interregional distribution across the brain. The only few regions where the models did not converge or gave poor estimates were generally small and noisy regions (e.g. subcallosal area, substantia nigra), and were present in comparable number among the two tracers. ^{11}C-ER176, however, displayed a higher V_T than ^{11}C-PBR28, both as an average value and at the individual level in each of the seven subjects.

The higher V_T of ^{11}C-ER176 is likely a reflection of its higher specific binding, as suggested by a higher BP_{ND}, a parameter that depends only on the amount of specific binding [23]. Notably, Fujita et al. reported lower V_T values for ^{11}C-ER176 than for ^{11}C-PBR28 in HAB subjects [32], but those values were derived from different populations of subjects, whereas our results are obtained from the same subjects scanned twice during the same day.

Importantly, for a similar plasma free fraction, the intersubject variability of the V_T values of ^{11}C-ER176 was smaller than that of ^{11}C-PBR28. Thanks to this smaller variability, clinical studies performed with ^{11}C-ER176 are expected to require fewer subjects. Considering, for example, a 30% increase of TSPO-binding in the temporal region of

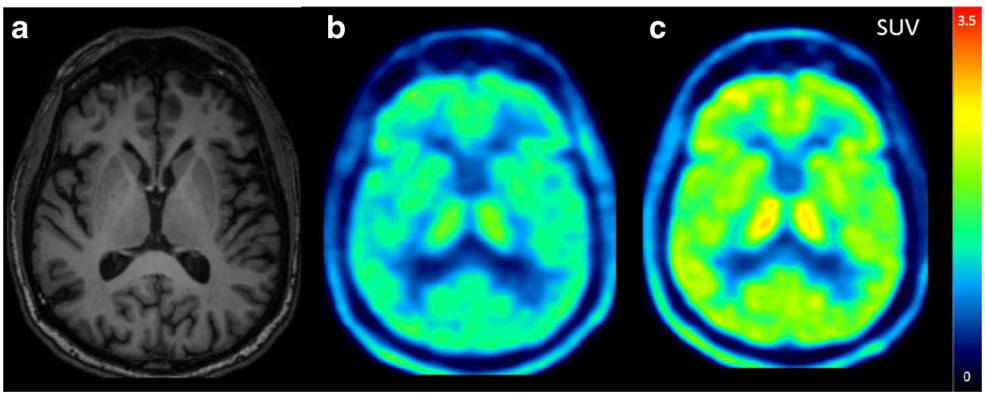

Fig. 2 Brain PET transaxial image in SUV scale of a mixed-affinity binder imaged with ^{11}C-PBR28 (**b**) and ^{11}C-ER176 (**c**), displayed along the corresponding MRI (**a**)

Table 1 Comparison of V_T values of ^{11}C-PBR28 and ^{11}C-ER176 using a two-tissue compartment model, and %COV values for each region

Region	*^{11}C-PBR28*		*^{11}C-ER176*	
	V_T (ml • cm^{-3})	*%COV*	V_T (ml • cm^{-3})	*%COV*
Sup frontal cortex	4.38 ± 2.01 (1.7%)	45.9	5.70 ± 1.43 (1.5%)	25.1
Post temporal cortex	4.28 ± 2.14 (1.8%)	50.0	5.77 ± 1.62 (1.6%)	28.1
Sup parietal cortex	4.21 ± 1.93 (2.0%)	45.8	5.43 ± 1.36 (2.0%)	25.0
Cerebellum	4.41 ± 2.16 (1.5%)	49.0	5.82 ± 1.51 (1.1%)	25.9

Representative brain regions from the right hemisphere. Values are mean ± SD. Average standard errors are listed in parentheses and are expressed as % of the variable itself

hypothetical patients with Alzheimer's disease (a figure in line with recent clinical findings [2]), and using the means and standard deviations of the temporal region reported in Table 1, we would need to study 45 subjects per group with ^{11}C-PBR28 and 15 subjects per group with ^{11}C-ER176 to be able to reject the null hypothesis that the population means of the experimental and control groups are equal, with power 0.8 and Type I error probability of 0.05.

Notably, our intersubject %COV values (Table 1) are somewhat higher than those commonly reported for HAB subjects, estimated at about 25% for most tracers [33]. However, our %COV values are calculated over a population that includes both HABs and MABs. Since the same subjects were scanned with both tracers, a correction for affinity was not needed. In addition, %COV values reflect the characteristics of the population under study. Our subjects were older volunteers, whose age range was 60 to 74. Since aging probably affects TSPO binding [34, 35], intersubject variability might also be increased to some extent.

We estimated the BP_{ND} values for ^{11}C-ER176 using a value of V_{ND} published in the literature and derived from pharmacological blockade [14], because we could not derive a plausible estimate from our population. For consistency, we used a value derived from the literature also for ^{11}C-PBR28, although we could successfully estimate our own value with the polymorphism plot and, to some extent, with the genomic plot despite a low correlation between mRNA and V_T values for HABs. The validity of the genomic plot relies on the strength of the correlation between mRNA and V_T values, and we previously showed that a correlation greater than $R^2 = 0.75$ is necessary to have a V_{ND} estimation with an acceptable bias [26]. In our subjects, the correlation was weaker for both HAB groups, and also the estimated V_{ND} value for ^{11}C-ER176 MABs was implausible despite a correlation of $R^2 = 0.74$. The polymorphism plot showed good linear fitting with ^{11}C-PBR28 data, and the estimation of V_{ND} yielded a very similar value to that reported in the literature (1.76 ml/cm^3 in our study and 1.98 ml/cm^3 from pharmacological blockade [31]), but the fitting for ^{11}C-ER176 was very poor and gave a value at odds with that known from studies with pharmacological blockade [14]. The failure of the ^{11}C-ER176 polymorphism plot, also noted by Ikawa et al. [14], can be ascribed to the small difference in binding between HABs (mean V_T value: 6.11 ml/cm^3) and MABs (5.47 ml/cm^3) — the respective values for ^{11}C-PBR28 are 5.60 and 3.55 ml/cm^3. Ikawa et al. hypothesized that the small binding difference could be due the fact that TSPO exists as a mixture of monomers, dimers, and higher-mers, and that most of the heteromers in MABs may maintain significant affinity for ^{11}C-ER176 [14]. In any case, ^{11}C-ER176 clearly has higher BP_{ND} than ^{11}C-PBR28: more than 4 times larger for HAB and more than 9 times larger for MABs. Our BP_{ND} differences closely match those reported by Fujita et al. who found that BP_{ND} of ^{11}C-ER176 was 3.5 times larger for HABs

Table 2 Comparison of microparameters of ^{11}C-PBR28 and ^{11}C-ER176 using a two-tissue compartment model in the same regions of Table 1

Region	K_1 (ml • cm^{-3} • min^{-1})		k_2 (min^{-1})		k_3 (min^{-1})		k_4 (min^{-1})	
	^{11}C-PBR28	*^{11}C-ER176*	*^{11}C-PBR28*	*^{11}C-ER176*	*^{11}C-PBR28*	*^{11}C-ER176*	*^{11}C-PBR28*	*^{11}C-ER176*
Sup frontal cortex	0.116 ± 0.028	0.141 ± 0.014	0.103 ± 0.037	0.070 ± 0.038	0.109 ± 0.059	0.131 ± 0.091	0.042 ± 0.012	0.081 ± 0.021
Post temporal cortex	0.131 ± 0.041	0.160 ± 0.019	0.110 ± 0.030	0.090 ± 0.049	0.089 ± 0.029	0.117 ± 0.089	0.039 ± 0.009	0.055 ± 0.013
Sup parietal cortex	0.118 ± 0.029	0.146 ± 0.016	0.090 ± 0.026	0.072 ± 0.032	0.077 ± 0.030	0.120 ± 0.118	0.040 ± 0.007	0.068 ± 0.018
Cerebellum	0.154 ± 0.040	0.187 ± 0.015	0.130 ± 0.026	0.104 ± 0.054	0.099 ± 0.034	0.135 ± 0.091	0.040 ± 0.011	0.063 ± 0.008

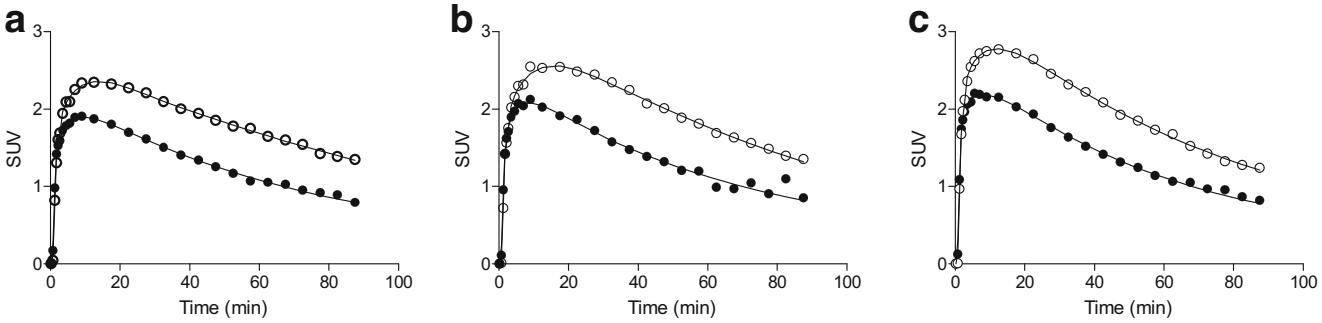

Fig. 3 Time–activity curves of three representative regions from the right hemisphere of a mixed-affinity binder: **a** posterior temporal, **b** putamen, and **c** cerebellum. Although both tracers exhibited a high uptake and fast wash-out, the SUV values of ^{11}C-ER176 (*white symbols*) were substantially higher than those of ^{11}C-PBR28 (*black symbols*). The *lines* represent fitting by a 2TCM

and 6.8 times larger for MABs, compared to that of ^{11}C-PBR28 [32].

^{11}C-ER176 has two additional advantages over ^{11}C-PBR28, which are known from the literature but were not further investigated in this study due to its design. The first one is the ability to image low-affinity binders. With ^{11}C-PBR28, LABs do not have sufficient signal to be imaged (and thus were excluded from the present study). However, studies with pharmacological blockade showed that the specific binding of ^{11}C-ER176 in LABs is even higher than the specific binding of ^{11}C-PBR28 in HABs [14]. While a statistical correction for genotype still needs to be performed, the use of ^{11}C-ER176 greatly simplifies the logistics of TSPO studies (the blood samples of the subjects can be genotyped all together at the end of the study) and makes it possible to include all subjects in research protocols, which is particularly important when studying rare diseases. The second advantage of ^{11}C-ER176 is the better time-stability of V_T. In this paper, the acquisitions were limited to 90 min for patients' comfort, but, contrarily to ^{11}C-PBR28 [36], the V_T of ^{11}C-ER176 is stable after 90 min, which suggests that no significant amount of radiometabolites enters the brain [14].

Finally, the present study has been performed on healthy volunteers, and may not directly reflect the relative behavior of the tracers under disease conditions. However, a higher specific binding at baseline is unlikely to translate into a disadvantage under disease. Moreover, some advantageous biological characteristics of ^{11}C-ER176, such as lower metabolism in plasma, better time-stability, and the possibility to image LABs, will be present under disease conditions as well.

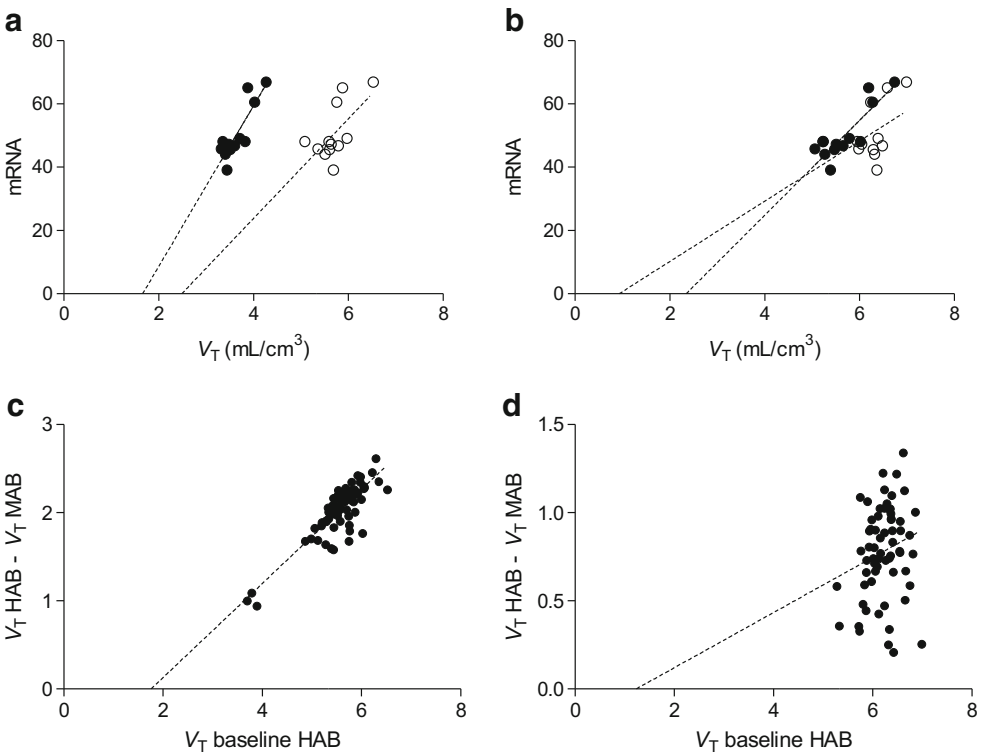

Fig. 4 Genomic plot for ^{11}C-PBR28 (**a**) and ^{11}C-ER176 (**b**) in HABs (*white symbols*) and MABs (*black symbols*). While the x-intercepts for ^{11}C-PBR28 gave a V_{ND} value of about 2 mL/cm^3, as it is expected, the V_{ND} estimation for ^{11}C-ER176 gave implausible values. Similarly, while the V_{ND} value derived with the polymorphism plot for ^{11}C-PBR28 compared favorably to that known from the literature (**c**), the fitting with ^{11}C-ER176 was poor and the resulting V_{ND} unreliable (**d**)

Table 3 V_T and BP_{ND} of ^{11}C-PBR28 and ^{11}C-ER176, and their ratio, in HABs and MABs

	V_T		BP_{ND}	
	HAB	*MAB*	*HAB*	*MAB*
^{11}C-PBR28	5.60 ± 2.44	3.55 ± 0.84	1.83 ± 1.23	0.79 ± 0.42
^{11}C-ER176	6.11 ± 1.91	5.47 ± 1.12	8.41 ± 2.93	7.41 ± 1.73
Ratio ^{11}C-ER176/^{11}C-PBR28	1.09	1.54	4.60	9.38

Conclusion

In this study, we found that ^{11}C-ER176 has a higher specific binding and a smaller intersubject variability compared to ^{11}C-PBR28. Thanks to these characteristics, clinical studies performed with ^{11}C-ER176 are expected to have higher statistical power and thus require fewer subjects. We conclude that ^{11}C-ER176 should be preferred over ^{11}C-PBR28 for TSPO studies in humans.

Funding This study was partially funded by the Harrison, Chao, Graham, and Nantz Funds of the Houston Methodist Foundation.

Compliance with ethical standards

Ethical approval All procedures performed in studies involving human participants were in accordance with the ethical standards of the institutional and/or national research committee and with the 1964 Helsinki Declaration and its later amendments or comparable ethical standards.

Informed consent Informed consent was obtained from all individual participants included in the study.

Conflict of interest Joseph Masdeu is on a General Electric Healthcare advisory board and receives research support from GE, Eli Lilly, Biogen, Abbvie, and Novartis. The other authors declare no conflict of interest.

Disclosure No potential conflicts of interest relevant to this article exist.

References

1. Cumming P, Burgher B, Patkar O, Breakspear M, Vasdev N, Thomas P, et al. Sifting through the surfeit of neuroinflammation tracers. J Cereb Blood Flow Metab. 2018;38:204–24.
2. Kreisl WC, Lyoo CH, McGwier M, Snow J, Jenko KJ, Kimura N, et al. In vivo radioligand binding to translocator protein correlates with severity of Alzheimer's disease. Brain. 2013;136:2228–38.
3. Richards EM, Zanotti-Fregonara P, Fujita M, Newman L, Farmer C, Ballard ED, et al. PET radioligand binding to translocator protein (TSPO) is increased in unmedicated depressed subjects. EJNMMI Res. 2018;8:57.
4. Plaven-Sigray P, Matheson GJ, Collste K, Ashok AH, Coughlin JM, Howes OD, et al. Positron emission tomography studies of the glial cell marker translocator protein in patients with psychosis: a meta-analysis using individual participant data. Biol Psychiatry. 2018;84:433–42.
5. Gershen LD, Zanotti-Fregonara P, Dustin IH, Liow JS, Hirvonen J, Kreisl WC, et al. Neuroinflammation in temporal lobe epilepsy measured using positron emission tomographic imaging of translocator protein. JAMA Neurol. 2015;72:882–8.
6. Narayan N, Owen DR, Mandhair H, Smyth E, Carlucci F, Saleem A, et al. Translocator protein as an imaging marker of macrophage and stromal activation in rheumatoid arthritis pannus. J Nucl Med. 2018;59:1125–32.
7. Roncaroli F, Su Z, Herholz K, Gerhard A, Turkheimer FE. TSPO expression in brain tumours: is TSPO a target for brain tumour imaging? Clin Translat Imaging. 2016;4:145–56.
8. Owen DR, Yeo AJ, Gunn RN, Song K, Wadsworth G, Lewis A, et al. An 18-kDa translocator protein (TSPO) polymorphism explains differences in binding affinity of the PET radioligand PBR28. J Cereb Blood Flow Metab. 2012;32:1–5.
9. Kreisl WC, Jenko KJ, Hines CS, Lyoo CH, Corona W, Morse CL, et al. A genetic polymorphism for translocator protein 18 kDa affects both in vitro and in vivo radioligand binding in human brain to this putative biomarker of neuroinflammation. J Cereb Blood Flow Metab. 2013;33:53–8.
10. Zanotti-Fregonara P, Pascual B, Rizzo G, Yu M, Pal N, Beers D, et al. Head-to-head comparison of (11)C-PBR28 and (18)F-GE180 for quantification of the translocator protein in the human brain. J Nucl Med. 2018;59:1260–6.
11. Zanotti-Fregonara P, Veronese M, Pascual B, Rostomily RC, Turkheimer F, Masdeu JC. The validity of (18)F-GE180 as a TSPO imaging agent. Eur J Nucl Med Mol Imaging. 2019;46(6):1205–7.
12. Fujita M, Imaizumi M, Zoghbi SS, Fujimura Y, Farris AG, Suhara T, et al. Kinetic analysis in healthy humans of a novel positron emission tomography radioligand to image the peripheral benzodiazepine receptor, a potential biomarker for inflammation. Neuroimage. 2008;40:43–52.
13. Zanotti-Fregonara P, Zhang Y, Jenko KJ, Gladding RL, Zoghbi SS, Fujita M, et al. Synthesis and evaluation of translocator 18 kDa protein (TSPO) positron emission tomography (PET) radioligands with low binding sensitivity to human single nucleotide polymorphism rs6971. ACS Chem Neurosci. 2014;5:963–71.
14. Ikawa M, Lohith TG, Shrestha S, Telu S, Zoghbi SS, Castellano S, et al. 11C-ER176, a radioligand for 18-kDa translocator protein, has adequate sensitivity to robustly image all three affinity genotypes in human brain. J Nucl Med. 2017;58:320–5.
15. Collste K, Forsberg A, Varrone A, Amini N, Aeinehband S, Yakushev I, et al. Test-retest reproducibility of [(11)C]PBR28 binding to TSPO in healthy control subjects. Eur J Nucl Med Mol Imaging. 2016;43:173–83.
16. Hammers A, Allom R, Koepp MJ, Free SL, Myers R, Lemieux L, et al. Three-dimensional maximum probability atlas of the human brain, with particular reference to the temporal lobe. Hum Brain Mapp. 2003;19:224–47.
17. Tonietto M, Rizzo G, Veronese M, Fujita M, Zoghbi SS, Zanotti-Fregonara P, et al. Plasma radiometabolite correction in dynamic PET studies: insights on the available modeling approaches. J Cereb Blood Flow Metab. 2016;36:326–39.
18. Gandelman MS, Baldwin RM, Zoghbi SS, Zea-Ponce Y, Innis RB. Evaluation of ultrafiltration for the free fraction determination of

single photon emission computed tomography (SPECT) tracers: ß-CIT, IBF, and iomazenil. J Pharm Sci. 1994;83:1014–9.
19. Abi-Dargham A, Gandelman M, Zoghbi SS, Laruelle M, Baldwin RM, Randall P, et al. Reproducibility of SPECT measurement of benzodiazepine receptors in human brain with [^{123}I]iomazenil. J Nucl Med. 1995;36:167–75.
20. Pajevic S, Daube-Witherspoon ME, Bacharach SL, Carson RE. Noise characteristics of 3-D and 2-D PET images. IEEE Trans Med Imaging. 1998;17:9–23.
21. Krzanowski WJ. Permutational tests for correlation matrices. Stat Comput. 1993;3:37–44.
22. Veronese M, Moro L, Arcolin M, Dipasquale O, Rizzo G, Expert P, et al. Covariance statistics and network analysis of brain PET imaging studies. Sci Rep. 2019;9(1):2496.
23. Innis RB, Cunningham VJ, Delforge J, Fujita M, Gjedde A, Gunn RN, et al. Consensus nomenclature for in vivo imaging of reversibly binding radioligands. J Cereb Blood Flow Metab. 2007;27:1533–9.
24. Lassen NA, Bartenstein PA, Lammertsma AA, Prevett MC, Turton DR, Luthra SK, et al. Benzodiazepine receptor quantification in vivo in humans using [11C]flumazenil and PET: application of the steady-state principle. J Cereb Blood Flow Metab. 1995;15:152–65.
25. Zanotti-Fregonara P, Xu R, Zoghbi SS, Liow JS, Fujita M, Veronese M, et al. The PET radioligand 18F-FIMX images and quantifies metabotropic glutamate receptor 1 in proportion to the regional density of its gene transcript in human brain. J Nucl Med. 2016;57:242–7.
26. Veronese M, Zanotti-Fregonara P, Rizzo G, Bertoldo A, Innis RB, Turkheimer FE. Measuring specific receptor binding of a PET radioligand in human brain without pharmacological blockade: the genomic plot. Neuroimage. 2016;130:1–12.
27. Guo Q, Colasanti A, Owen DR, Onega M, Kamalakaran A, Bennacef I, et al. Quantification of the specific translocator protein signal of 18F-PBR111 in healthy humans: a genetic polymorphism effect on in vivo binding. J Nucl Med. 2013;54:1915–23.
28. Rizzo G, Veronese M, Heckemann RA, Selvaraj S, Howes OD, Hammers A, et al. The predictive power of brain mRNA mappings for in vivo protein density: a positron emission tomography correlation study. J Cereb Blood Flow Metab. 2014;34(5):827–35.
29. Hawrylycz MJ, Lein ES, Guillozet-Bongaarts AL, Shen EH, Ng L, Miller JA, et al. An anatomically comprehensive atlas of the adult human brain transcriptome. Nature. 2012;489:391–9.
30. Rizzo G, Veronese M, Expert P, Turkheimer FE, Bertoldo A. MENGA: a new comprehensive tool for the integration of neuroimaging data and the Allen human brain transcriptome atlas. PLoS One. 2016;11:e0148744.
31. Owen DR, Guo Q, Kalk NJ, Colasanti A, Kalogiannopoulou D, Dimber R, et al. Determination of [(11)C]PBR28 binding potential in vivo: a first human TSPO blocking study. J Cereb Blood Flow Metab. 2014;34:989–94.
32. Fujita M, Kobayashi M, Ikawa M, Gunn RN, Rabiner EA, Owen DR, et al. Comparison of four (11)C-labeled PET ligands to quantify translocator protein 18 kDa (TSPO) in human brain: (R)-PK11195, PBR28, DPA-713, and ER176-based on recent publications that measured specific-to-non-displaceable ratios. EJNMMI Res. 2017;7:84.
33. Owen DR, Guo Q, Rabiner EA, Gunn RN. The impact of the rs6971 polymorphism in TSPO for quantification and study design. Clin Translat Imaging. 2015;3:417–22.
34. Paul S, Gallagher E, Liow JS, Mabins S, Henry K, Zoghbi SS, et al. Building a database for brain 18 kDa translocator protein imaged using [(11)C]PBR28 in healthy subjects. J Cereb Blood Flow Metab. 2018:271678x18771250 [Epub ahead of print].
35. Tuisku J, Plaven-Sigray P, Gaiser EC, Airas L, Al-Abdulrasul H, Bruck A, et al. Effects of age, BMI and sex on the glial cell marker TSPO - a multicentre [11C]PBR28 HRRT PET study. bioRxiv. 2019:564831.
36. Rizzo G, Veronese M, Tonietto M, Zanotti-Fregonara P, Turkheimer FE, Bertoldo A. Kinetic modeling without accounting for the vascular component impairs the quantification of [(11)C]PBR28 brain PET data. J Cereb Blood Flow Metab. 2014;34:1060–9.